



Accelerating the 3D $T_{1\rho}$ mapping of cartilage using a signal-compensated robust tensor principal component analysis model

Yuanyuan Liu^{1,2,3,4}, Leslie Ying⁵, Weitian Chen⁶, Zhuo-Xu Cui⁴, Qingyong Zhu⁴, Xin Liu¹, Hairong Zheng¹, Dong Liang^{1,4}, Yanjie Zhu¹

¹Paul C. Lauterbur Research Center for Biomedical Imaging, Shenzhen Institute of Advanced Technology, Chinese Academy of Sciences, Shenzhen, China; ²National Innovation Center for Advanced Medical Devices, Shenzhen, China; ³Shenzhen College of Advanced Technology, University of Chinese Academy of Sciences, Shenzhen, China; ⁴Research Center for Medical AI, Shenzhen Institute of Advanced Technology, Chinese Academy of Sciences, Shenzhen, China; ⁵Department of Biomedical Engineering and Department of Electrical Engineering, University at Buffalo, The State University of New York, Buffalo, New York, USA; ⁶Department of Imaging and Interventional Radiology, The Chinese University of Hong Kong, Shatin, Hong Kong, China

Contributions: (I) Conception and design: Y Liu, Y Zhu; (II) Administrative support: D Liang; (III) Provision of study materials or patients: D Liang; (IV) Collection and assembly of data: Y Liu; (V) Data analysis and interpretation: Y Liu, Y Zhu; (VI) Manuscript writing: All authors; (VII) Final approval of manuscript: All authors.

Correspondence to: Dong Liang, PhD; Yanjie Zhu, PhD. Paul C. Lauterbur Research Center for Biomedical Imaging, Shenzhen Institute of Advanced Technology, Chinese Academy of Sciences, Shenzhen 518055, China. Email: dong.liang@siat.ac.cn; yj.zhu@siat.ac.cn.

Background: Magnetic resonance (MR) quantitative $T_{1\rho}$ imaging has been increasingly used to detect the early stages of osteoarthritis. The small volume and curved surface of articular cartilage necessitate imaging with high in-plane resolution and thin slices for accurate $T_{1\rho}$ measurement. Compared with 2D $T_{1\rho}$ mapping, 3D $T_{1\rho}$ mapping is free from artifacts caused by slice cross-talk and has a thinner slice thickness and full volume coverage. However, this technique needs to acquire multiple $T_{1\rho}$ -weighted images with different spin-lock times, which results in a very long scan duration. It is highly expected that the scan time can be reduced in 3D $T_{1\rho}$ mapping without compromising the $T_{1\rho}$ quantification accuracy and precision.

Methods: To accelerate the acquisition of 3D $T_{1\rho}$ mapping without compromising the $T_{1\rho}$ quantification accuracy and precision, a signal-compensated robust tensor principal component analysis method was proposed in this paper. The 3D $T_{1\rho}$ -weighted images compensated at different spin-lock times were decomposed as a low-rank high-order tensor plus a sparse component. Poisson-disk random undersampling patterns were applied to k-space data in the phase- and partition-encoding directions in both retrospective and prospective experiments. Five volunteers were involved in this study. The fully sampled k-space data acquired from 3 volunteers were retrospectively undersampled at $R=5.2$, 7.7 , and 9.7 , respectively. Reference values were obtained from the fully sampled data. Prospectively undersampled data for $R=5$ and $R=7$ were acquired from 2 volunteers. Bland-Altman analyses were used to assess the agreement between the accelerated and reference $T_{1\rho}$ measurements. The reconstruction performance was evaluated using the normalized root mean square error and the median of the normalized absolute deviation (MNAD) of the reconstructed $T_{1\rho}$ -weighted images and the corresponding $T_{1\rho}$ maps.

Results: $T_{1\rho}$ parameter maps were successfully estimated from $T_{1\rho}$ -weighted images reconstructed using the proposed method for all accelerations. The accelerated $T_{1\rho}$ measurements and reference values were in good agreement for $R=5.2$ ($T_{1\rho}$: 40.4 ± 1.4 ms), $R=7.7$ ($T_{1\rho}$: 40.4 ± 2.1 ms), and $R=9.7$ ($T_{1\rho}$: 40.9 ± 2.2 ms) in the Bland-Altman analyses. The $T_{1\rho}$ parameter maps reconstructed from the prospectively undersampled data also showed promising image quality using the proposed method.

Conclusions: The proposed method achieves the 3D $T_{1\rho}$ mapping of *in vivo* knee cartilage in eight minutes using a signal-compensated robust tensor principal component analysis method in image reconstruction.

Keywords: 3D $T_{1\rho}$; cartilage; signal compensated; robust tensor principal component analysis; tensor decomposition

Submitted Jun 24, 2020. Accepted for publication Apr 19, 2021.

doi: 10.21037/qims-20-790

View this article at: <http://dx.doi.org/10.21037/qims-20-790>

Introduction

Osteoarthritis (OA) is an important public health problem (1,2). Cartilage degeneration due to OA changes the functional properties of cartilage and can eventually cause cartilage destruction (3). Conventional magnetic resonance imaging (MRI) provides sufficient tissue contrast to detect morphological changes in cartilage (4) but cannot measure the physiological changes in cartilage that occur during the earliest stages of OA development (2,5). Recent studies have shown that quantitative MRI has the potential to serve as a reproducible, noninvasive biomarker to identify subjects at risk for OA (6,7).

Magnetic spin-lattice relaxation in the rotating frame ($T_{1\rho}$) has received considerable interest in the early detection of cartilage degeneration (8,9). It can probe the slow motion of the macromolecules in the articular cartilage extracellular matrix (ECM). Changes to the ECM, such as proteoglycan loss, can be reflected in the $T_{1\rho}$ measurements (10). *In vivo* studies have shown that the cartilage $T_{1\rho}$ value increased in OA subjects compared with controls (11-13). Furthermore, elevated $T_{1\rho}$ was observed in subcompartments in OA subjects where no obvious morphological changes were observed, suggesting the capability of $T_{1\rho}$ in detecting very early biochemical changes within the cartilage matrix (12).

Quantitative $T_{1\rho}$ imaging suffers from a long scan time since multiple $T_{1\rho}$ -weighted images with different spin-lock times (TSLs) must be acquired to calculate the $T_{1\rho}$ values. Relative to 2D $T_{1\rho}$ mapping, 3D $T_{1\rho}$ mapping is more suitable for cartilage imaging because of the small size of the articular cartilage. However, using 3D imaging further prolongs the scan time and thus limits the widespread clinical use of this technique. Therefore, it is necessary to accelerate the data acquisition for 3D $T_{1\rho}$ mapping of cartilage.

Several methods based on compressed sensing (CS) have been proposed for 3D $T_{1\rho}$ mapping acceleration (14-19). Due to the high compressibility of the image in the parametric direction, CS is especially suitable for $T_{1\rho}$ mapping. Pandit *et al.* combined CS with data-driven

parallel imaging (PI) to accelerate cartilage $T_{1\rho}$ mapping and successfully implemented the data acquisition process on a clinical MRI scanner. The scan time was reduced to one-third that associated with full sample acquisition (14). Zhou *et al.* reconstructed the undersampled $T_{1\rho}$ mapping data using the combined CS and PI method and achieved acceleration factors of 3 and 3.5. However, this technique has been applied only in a 2D version of the reconstruction scheme (18). Zibetti *et al.* compared the results with reconstructions of 3D $T_{1\rho}$ images based on CS using different regularization functions and achieved a very high acceleration factor of 10 for both Cartesian and radial acquisitions (16,19). They recommended the low-rank plus sparse matrix decomposition method (L+S) (20) for the Cartesian acquisition, one of the most popular methods due to its excellent reconstruction performance (16). Although these studies showed promising results using retrospectively undersampled data, no prospective undersampling reconstruction was shown.

Recently we developed an accelerated 2D $T_{1\rho}$ mapping method, which is referred to as SCOPE, and applied it for 2D $T_{1\rho}$ mapping of brain (21). A signal compensation strategy is applied in SCOPE to enhance the low rankness of the $T_{1\rho}$ -weighted image matrix and reconstruct images using the L+S method (20) followed by the inverse compensation. SCOPE needs to vectorize 2D images to construct the image matrix. The vectorization step leads to the loss of spatial information and may cause reconstruction degradation (22). When extending SCOPE to 3D $T_{1\rho}$ mapping, high-dimensional data can be treated as a tensor to avoid vectorizing the 3D images. This tensor-based representation has been successfully applied in dynamic MRI (22,23); it utilizes the spatial coherence of the image and, hence, can improve the reconstruction performance.

In this study, we investigated the feasibility of a signal-compensated robust tensor principal component analysis (TenSCOPE) method for accelerated 3D cartilage $T_{1\rho}$ mapping. In this framework, we decompose the 3D $T_{1\rho}$ -weighted images compensated at different TSLs as a low-rank high-order tensor plus sparse component. Both

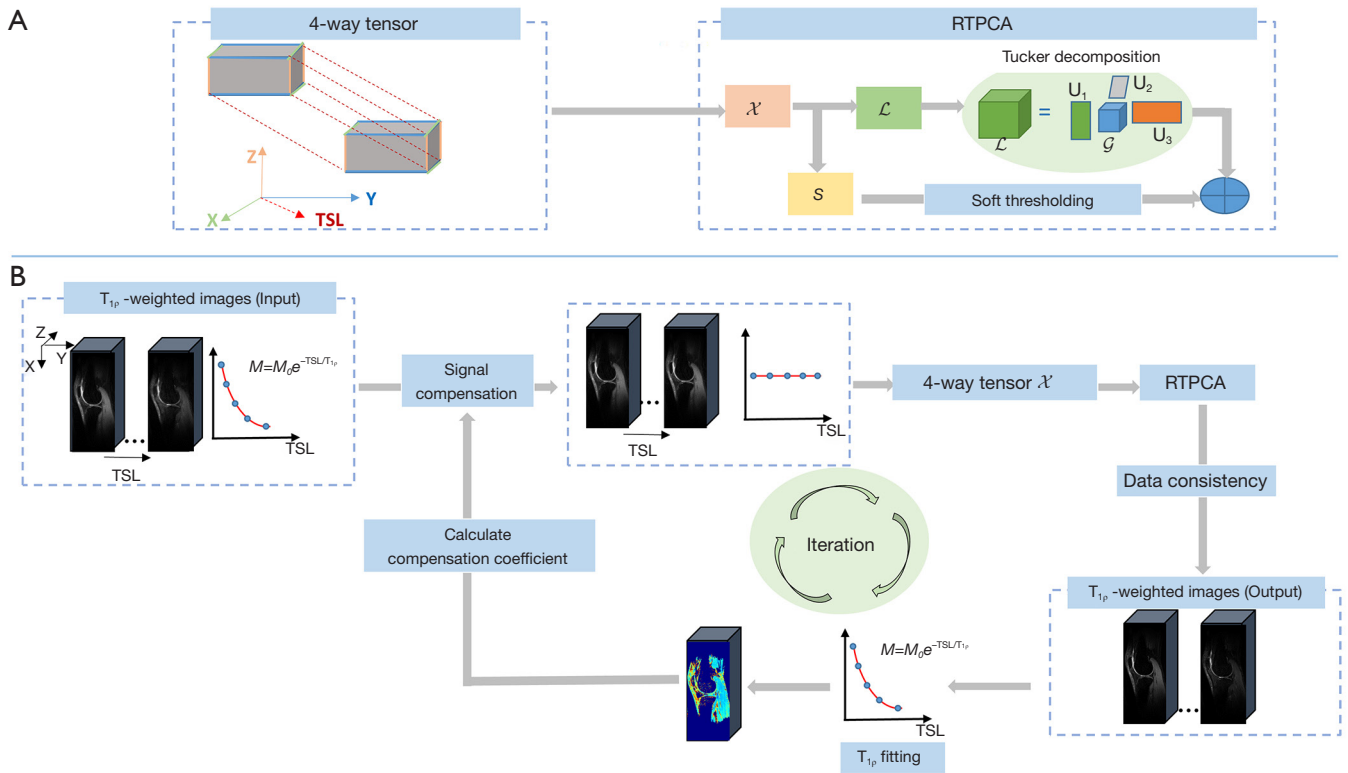


Figure 1 Flow diagram of the robust tensor principal component analysis (RTPCA) model and the TenSCOPE method for image reconstruction. (A) The RTPCA model. (B) The TenSCOPE method for image reconstruction. Note that the 4-way tensor and Tucker decompositions are shown for illustration purposes only.

retrospective and prospective experiments were performed to assess the performance of TenSCOPE.

Methods

Robust tensor principal component analysis (RTPCA) model

The T_{1ρ}-weighted image matrix can be decomposed as a superposition of a sparse component \mathcal{S} and a low-rank tensor \mathcal{L} . The corresponding optimization model is defined using the following formula:

$$\min_{\{\mathcal{X}, \mathcal{L}, \mathcal{S}\}} \mathcal{R}ank(\mathcal{L}) + \mathcal{G}(\mathcal{S}) \text{ s.t. } \mathcal{X} = \mathcal{L} + \mathcal{S}, \mathcal{Y} = \mathcal{A}(\mathcal{X}) + \mathcal{E} \quad [1]$$

where $\mathcal{X} \in \mathfrak{R}^{N_1 \times N_2 \times N_3 \times N_{TSL}}$ is the image series to be reconstructed and $\mathcal{Y} \in \mathfrak{R}^{N_1 \times N_2 \times N_3 \times N_{TSL} \times N_c}$ represents the acquired k-space data. N_1 , N_2 , and N_3 represent the number of frequency- and phase-encoding lines in k_x , k_y , and k_z , respectively. N_{TSL} is the total number of TSLs,

and N_c represents the channel number. \mathcal{G} denotes the sparse representation operator. \mathcal{A} represents the multicoil encoding operator which performs the multiplication with coil sensitivities followed by the undersampled Fourier transform (20,24). \mathcal{E} is the measurement error.

The rank of the tensor \mathcal{L} needs to be minimized. However, unlike matrix rank, the definition of tensor rank depends on the decomposition methods, which is not unique (25,26). Generally, a tensor can be decomposed as the sum of several rank-1 tensors. Tensor rank is based on the number of rank-1 tensors. We used Tucker decomposition in this work as a generalization of the matrix singular-value decomposition (SVD) in the high-dimensional space that is computationally tractable and flexible (27). Specifically, this process decomposes a tensor into the multiplication between a core tensor and matrices along each mode, which is similar to the SVD of matrices, as shown in Figure 1A. A demonstration of Tucker decomposition is shown in Algorithm 1. The rank of the tensor in mode i of unfolding is defined as:

$$\text{rank}_i(\mathcal{L}) = \text{rank}(\mathcal{L}_i) \tag{2}$$

where \mathcal{L}_i represents the mode- i matricization of tensor \mathcal{L} , which can be defined as $\mathcal{L}_i = \text{unfold}(\mathcal{L}, i)$ (26). The i -rank can be regarded as a generalization of the SVD rank (for a matrix, these two are equivalent). With this definition, a low rank tensor is a tensor with all low rank unfoldings. Therefore, to estimate low-rank tensors, the multi-dimensional tensor trace norm of an i -order tensor is calculated using the weighted sum of the nuclear norms of the unfoldings in each mode:

$$\|\mathcal{L}\|_* = \sum_{i=1}^n \lambda_i \|\mathcal{L}_i\|_* \tag{3}$$

where $\lambda = [\lambda_1, \lambda_2, \dots, \lambda_n]^T$ represents the rank regularization parameters of different unfolding matrices for the Tucker nuclear norm. With the above tensor rank definition, Eq. [1] can be reformulated as:

$$\min_{\{\mathcal{X}, \mathcal{L}, \mathcal{S}\}} \|\mathcal{L}\|_* + \Theta(\mathcal{S}) \text{ s.t. } \mathcal{X} = \mathcal{L} + \mathcal{S}, \mathcal{Y} = \mathcal{A}(\mathcal{X}) + \mathcal{E} \tag{4}$$

Algorithm 1 Tucker Decomposition Algorithm for TenSCOPE reconstruction

INPUT: 4-way data tensor \mathcal{L} with dimensions $(N_1, N_2, N_3, N_{\text{TSL}})$ and the rank regularization parameter $\lambda = [\lambda_1, \lambda_2, \lambda_3, \lambda_4]$

ALGORITHM:

- (1) Unfold the tensor \mathcal{L} along its single modes:
 - \mathcal{L}_1 : which reshapes \mathcal{L} into a $N_1 \times (N_2 N_3 N_{\text{TSL}})$ complex matrix
 - \mathcal{L}_2 : which reshapes \mathcal{L} into a $N_2 \times (N_1 N_3 N_{\text{TSL}})$ complex matrix
 - \mathcal{L}_3 : which reshapes \mathcal{L} into a $N_3 \times (N_1 N_2 N_{\text{TSL}})$ complex matrix
 - \mathcal{L}_4 : which reshapes \mathcal{L} into a $N_{\text{TSL}} \times (N_1 N_2 N_3)$ complex matrix
- (2) Compute the complex SVD of \mathcal{L}_n and obtain the orthogonal matrices $U^{(1)}, U^{(2)}, U^{(3)}$, and $U^{(4)}$ from the n^{th} -mode signal subspace
- (3) Compute the complex core tensor \mathcal{G} related by

$$\mathcal{G} = \mathcal{L} \times_1 U_{(1)}^H \times_2 U_{(2)}^H \times_3 U_{(3)}^H \times_4 U_{(4)}^H$$

which is equivalent to its unfolding forms:

$$\mathcal{G}_n = U_{(n)}^H \mathcal{L}_n \left[U_{(i)} \otimes U_{(j)} \right] \text{ with } 1 \leq n \leq 4 \text{ and } i \neq j \neq n$$

where \otimes denotes the Kronecker product

- (4) Compute the high-order singular value truncation (hard-thresholding):
rank(\mathcal{G}_n) = λ_n with $1 \leq n \leq 4$

- (5) Construct back the filtered tensor $\mathcal{L}_n^{\text{den}}$:

$$\mathcal{L}_n^{\text{den}} = U_{(n)} \mathcal{G}_n \left[U_{(i)} \otimes U_{(j)} \right]^H \text{ with } 1 \leq n \leq 4 \text{ and } i \neq j \neq n$$

OUTPUT: The denoised tensor \mathcal{L}^{den} is obtained by folding.

TenSCOPE model

In TenSCOPE, a signal compensation strategy is applied

by multiplying the $T_{1\rho}$ -weighted image signal by the compensation coefficient. The compensation coefficient can be calculated via the inversion of the $T_{1\rho}$ decay using the following formula:

$$\text{Coef}_k = 1 / \exp\left(-\text{TSL}_k / T_{1\rho}\right)_{k=1,2,\dots,N_{\text{TSL}}} \tag{5}$$

where TSL_k represents the spin-lock duration for the k^{th} $T_{1\rho}$ -weighted image, and N_{TSL} is the total TSL number. The compensated $T_{1\rho}$ -weighted images are then obtained with the RTPCA model. The optimization model of the TenSCOPE method is defined as follows:

$$\min_{\{\mathcal{X}, \mathcal{L}, \mathcal{S}\}} \|\mathcal{L}\|_* + \Theta(\mathcal{S}) \text{ s.t. } \mathcal{C}(\mathcal{X}) = \mathcal{L} + \mathcal{S}, \mathcal{Y} = \mathcal{A}(\mathcal{X}) + \mathcal{E} \tag{6}$$

where $\mathcal{C}(\cdot)$ denotes the pixelwise signal compensation operator using the above compensation coefficients Coef_k (21). The signal intensity of the image matrix in the TSL direction should be the same after applying the signal compensation, and the rank of \mathcal{L} will then decrease.

The solution strategy for Eq. [6] is summarized in Algorithm 2 and depicted in Figure 1B. First, the $T_{1\rho}$ -weighted image series to be reconstructed is involved in signal compensation. Low-resolution $T_{1\rho}$ maps are reconstructed using the fully sampled k-space center to estimate the initial compensation coefficient. Specifically, the compensation was performed by multiplying the original image signal by the inversion of the monoexponential decay at each voxel. Then, the image series represented by a 4-way tensor \mathcal{X} were decomposed by a low-rank tensor \mathcal{L} and a sparse component \mathcal{S} . \mathcal{L} and \mathcal{S} were obtained using Tucker decomposition [denoted by $\mathcal{T}(\cdot)$] and soft thresholding [denoted by $\mathcal{D}(\cdot)$], respectively, to reconstruct the $T_{1\rho}$ -weighted images. Soft thresholding is defined as follows:

$$\begin{cases} \mathcal{D}(\mathcal{S}_i) = \text{fold}\left(\text{ST}\left(\text{unfold}(\mathcal{S}, i)\right)\right) \\ \text{ST}(p) = \frac{p}{|p|} \max(0, |p| - v) \end{cases} \tag{7}$$

where $\text{unfold}(\mathcal{S}, i)$ represents the mode- i matricization of tensor \mathcal{S} ; $\text{fold}(\cdot)$ represents the inverse process, which folds a matrix to a tensor; p is an element of the image matrix; v represents the threshold. In the j -th iteration, the data consistency is enforced by $\mathcal{L}_j + \mathcal{S}_j - \mathcal{C}(\mathcal{A}^*(\mathcal{A}C^{-1}(\mathcal{L}_j + \mathcal{S}_j) - \mathcal{Y}))$, where $C^{-1}(\cdot)$ represents the division of the image signal by the compensation coefficient in Eq. [5] pixel by pixel. \mathcal{A}^* is the adjoint operation of \mathcal{A} , which performs the backward function (21,24). The reconstructed $T_{1\rho}$ -weighted images are then used to update the $T_{1\rho}$ maps with the exponential model,

and are applied to update the compensation coefficient. The image reconstruction and compensation coefficient updating steps are repeated alternately until the algorithm convergence is reached. The stopping criterion in this method is defined as the point when the algorithm reaches the maximum number of iterations or at which the relative change in the solutions in two consecutive iterations is less than a predefined value.

Algorithm 2 The pseudocode of the proposed TenSCOPE algorithm

INPUTS: \mathcal{A} : encoding operator

\mathcal{Y} : the undersampled k-space data

TSL_k: the kth spin-lock duration

OUTPUTS: \mathcal{X} : the reconstructed image series

1. Initialize $\mathcal{X}^0 = \mathcal{A}^*(\mathcal{Y})$ and the initial T_{1ρ} map T_{1ρ}⁰
 2. For the outer iteration $i = 1:I$, perform the following steps until convergence
 - [1] Calculate $\text{Coef}^i = 1/\exp(-\text{TSL}_k / T_{1\rho}^{i-1})_{k=1,2,\dots,N_{\text{TSL}}}$
 - [2] $\mathcal{U}_0^i = C(\mathcal{X}^{i-1})$ with Coefⁱ
 - [3] Initialize $S_0 = 0$
 - [4] For the inner iteration $j = 1:J$, perform the following steps
 - a. update \mathcal{L}_j by Tucker decomposition, $\mathcal{L}_j = \mathcal{T}(\mathcal{U}_{j-1}^i - S_{j-1})$
 - b. update S_j by soft thresholding, $S_j = \mathcal{D}(\mathcal{X}_{j-1}^i - \mathcal{L}_j)$
 - c. Data consistency $\mathcal{U}_j^i = \mathcal{L}_j + S_j - C(\mathcal{A}^*(\mathcal{A}C^{-1}(\mathcal{L}_j + S_j) - \mathcal{Y}))$
 - [5] End the inner iteration
 - [6] $\mathcal{X}^i = C^{-1}(\mathcal{U}_j^i)$
 - [7] Update T_{1ρ}ⁱ
-

T_{1ρ} map estimation

T_{1ρ} maps are obtained by fitting the reconstructed T_{1ρ}-weighted images with different TSLs pixel by pixel:

$$M_k = M_0 \exp(-\text{TSL}_k / T_{1\rho})_{k=1,2,\dots,N_{\text{TSL}}} \quad [8]$$

where M_0 is the baseline image intensity without applying a spin-lock pulse and M_k is the signal intensity for the k th TSL image. During reconstruction, a log-based linear fitting method was used to update the T_{1ρ} map and reduce the calculation complexity (21). The final T_{1ρ} map was estimated using the nonlinear least-squares fitting method with the Levenberg-Marquardt algorithm from the reconstructed T_{1ρ}-weighted images.

Data acquisition and reconstruction

All the MR scans were performed on a 3T scanner (uMR

790, United Imaging Healthcare, Shanghai, China) using a commercial 12-channel phased-array knee coil. T_{1ρ}-weighted image datasets of the knee were acquired using a 3D modulated flip angle technique in refocused imaging with an extended echo train (MATRIX) sequence and a self-compensated paired spin-lock preparation pulse (28). The spin-lock frequency was fixed at 500 Hz (B₁ of spin-lock pulse = 11.74 μT). Three healthy volunteers (1 male, age: 26 years old; 2 females, age: 45±15 years old) were recruited for T_{1ρ} scanning. The imaging parameters were: TE/TR = 8.96/2,000 ms, matrix size: 256×146×124, pixel size = 0.98×0.98×1 mm³, echo train length = 60, echo spacing = 4.48 ms, and TSLs = 5, 10, 20, 40, and 60 ms. The scan time for the fully sampled dataset with elliptical scanning was 39 minutes and 30 seconds. The fully sampled k-space datasets were retrospectively undersampled using Poisson-disk random (15,18) patterns with R=5.2, 7.7, and 9.7. The sampling masks for each TSL are different. Figures 2 and 3 show the applied undersampling pattern of ky-kz for R=5.2 and R=9.7. Data were fully sampled in the frequency encoding direction. To estimate the coil sensitivity map, the central k-space area was fully sampled with size = 16×16 for R=5.2 and R=7.7 and size = 12×12 for R=9.7. Furthermore, the T_{1ρ} mapping data were prospectively undersampled using the Poisson-disk randomly undersampled scheme with net acceleration factors R=5 and R=7. Two volunteers (one male, 29 years old; one female, 30 years old) were involved in the prospective study. The imaging parameters were the same as those used in the retrospective experiment. The scan time was 10 minutes and 10 seconds for R=5 and 7 minutes and 20 seconds for R=7. Due to the time limit, the reference scan was acquired using the PI with accelerating factor R=3. The reference images were then reconstructed using the ESPIRiT method (29) from the BART toolbox (download link: <https://people.eecs.berkeley.edu/~mlustig/Software.html>). The scan time for the reference scan was 18 minutes and 50 seconds.

The TenSCOPE method was applied to reconstruct the 3D T_{1ρ}-weighted image series. In the retrospective reconstruction, the iteration numbers of the outer loop were 4, 5, and 6 for R=5.2, 7.7, and 9.7 respectively. For the inner loop, the corresponding iteration numbers were 16, 18, and 20. In the prospective reconstruction, the iteration numbers for R=5 and 7 were 4 and 5 for the outer loop and 16 and 20 for the inner loop, respectively. All the tensor transforms and decompositions were implemented using the MATLAB tensor toolbox by Brett *et al.* from Sandia National Laboratories (download link: <http://www>.

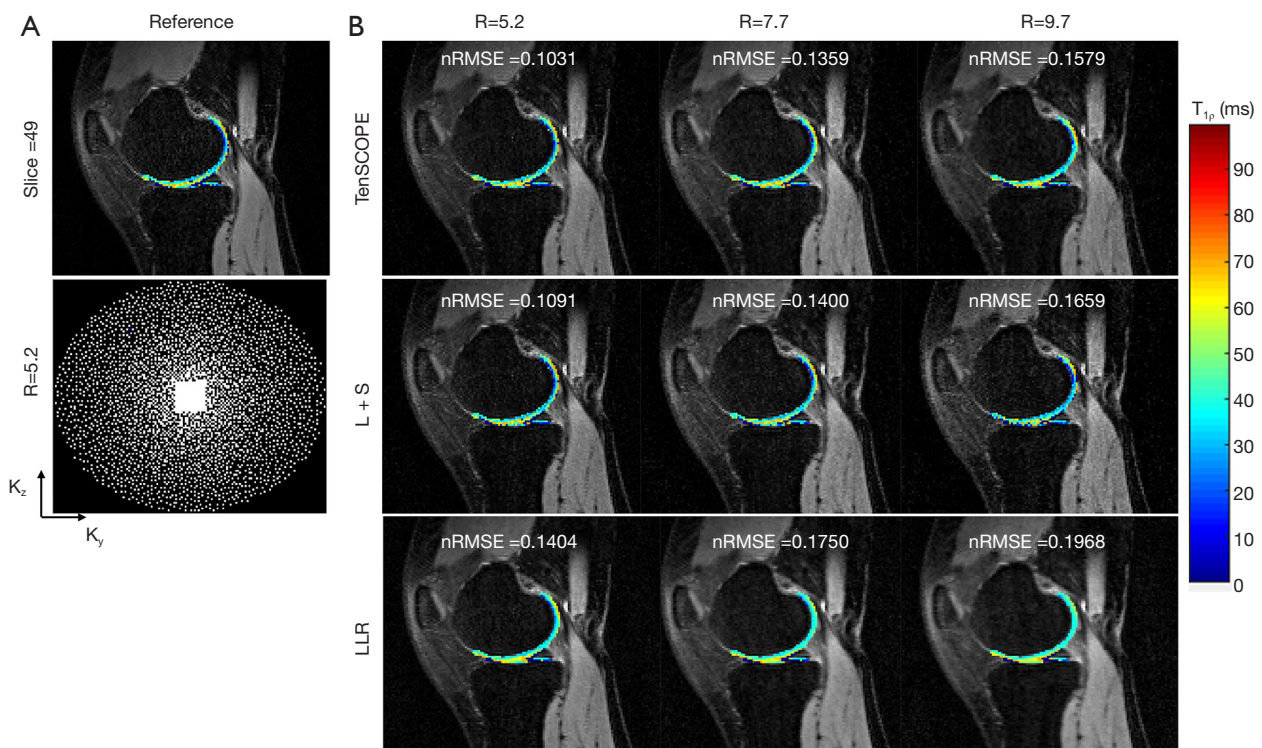


Figure 2 The undersampling pattern and estimated $T_{1\rho}$ parameter maps for selected cartilage ROIs. (A) The 2D Poisson-disk random undersampling pattern in k_y - k_z for a net acceleration factor of $R=5.2$. (B) The estimated $T_{1\rho}$ parameter maps for selected cartilage ROIs overlaid on the reconstructed $T_{1\rho}$ -weighted images at TSL = 5 ms for $R=5.2$, 7.7, and 9.7 using the TenSCOPE, L+S, and LLR methods, respectively, for slice 49 of subject 1. The reference image and $T_{1\rho}$ parameter map were obtained from the fully sampled k-space data.

tensortoolbox.org/). In this study, 4 parameters needed to be tuned in the Tucker decomposition, and the reconstruction quality depends on 3 rank constraint parameters that control the complexity of spatial redundancy and 1 rank constraint parameter that controls the complexity of temporal redundancy in Tucker decomposition. The spatial redundancy parameters are chosen empirically as $0.45\times$ the number of frequency-encoding lines, $0.65\times$ the number of phase-encoding lines, and $0.65\times$ the number of partition-encoding lines (30). Since signal compensation enhances the low rankness of the image matrix in the parameter direction, the temporal redundancy parameter is set as 1. The threshold in soft thresholding for different TSLs was set as [0.02, 0.02, 0.025, 0.025, 0.03]. For comparison, the L+S method (20) and the locally low-rank method (LLR) (31) were also applied to reconstruct the undersampled k-space data. In the L+S method, the singular-value thresholding and soft-thresholding algorithms (20) were used to solve for the L component and S component, respectively. The ratio for singular-value thresholding was set as 0.02, and the ratio

for soft thresholding was set as [0.02, 0.025, 0.025, 0.035, 0.035] to achieve optimal performance. In the LLR method, the iteration number was set as 40, 50, and 60 for $R=5.2$, 7.7, and 9.7, respectively. The block size was set as 8×8 , and the threshold for the singular value decomposition was initially set as 0.03 of the largest singular value, reduced to 0.01 after 10 iterations, and finally reduced to 0.005 in the final 10 iterations.

Assessment

The quality of the reconstructed $T_{1\rho}$ -weighted images was assessed based on the normalized root mean square error (nRMSE) using the following formula:

$$\text{nRMSE} = \sqrt{\frac{\|x_{\text{est}} - x_{\text{ref}}\|_2^2}{\|x_{\text{ref}}\|_2^2}} \quad [9]$$

where x_{est} is the reconstructed image from the undersampled k-space data, x_{ref} denotes the reference image from the fully sampled data.

The T_{1ρ} quantification was assessed using the median of the normalized absolute deviation (MNAD) (16) and the mean T_{1ρ} values (18) from the accelerated reconstruction for all the pixels in the selected cartilage regions of interest (ROIs) from all the acquisitions. In addition, three ROIs in the cartilage region were manually selected from four slices of each dataset (a total of 36 ROIs), and the mean T_{1ρ} values were calculated for each ROI. Cartilage was segmented manually according to Li *et al.*'s work (12). Linear regression and Bland-Altman analysis were used to assess the agreement of the T_{1ρ} parameter between the accelerated reconstructions and the reference.

The MNAD was defined as:

$$\text{MNAD(ROI)} = \text{Median}_{m \in \text{ROI}} \left(\frac{|p(m) - p_{\text{ref}}(m)|}{(p(m) + p_{\text{ref}}(m))/2} \right) \quad [10]$$

where $p_{\text{ref}}(m)$ represents the reference parameter from fully sampled data; $p(m)$ represents the T_{1ρ} parameter estimated from the reconstructed images of the undersampled data. An MNAD of 0.1 corresponds to a median deviation of 10% from the estimated parameters compared with the reference.

The mean T_{1ρ} value of the selected ROI compartment was defined as follows:

$$\bar{T}_{1\rho} = \frac{1}{N} \sum_{n=1}^N T_{1\rho}^{(n)} \quad [11]$$

where N represents the number of pixels in the selected ROI compartment, $\bar{T}_{1\rho}$ represents the mean T_{1ρ} value of the selected ROI compartment, and $T_{1\rho}^{(n)}$ represents the T_{1ρ} value of the nth pixel of the selected ROI compartment.

In the prospective experiments, the T_{1ρ} values of the selected ROIs in cartilage regions from the 2 subjects were also calculated and then compared with the reference values by the Wilcoxon signed-rank test. Statistical significance was set to $P < 0.05$.

All the image reconstructions and analyses were performed in MATLAB 2017b (The MathWorks, Natick, MA, USA) on an HP workstation with 160 GB DDR4 RAM and 32 cores (two 16-core Intel Xeon E5-2660 2.6 GHz processors).

The study was conducted in accordance with the Declaration of Helsinki (as revised in 2013). The study was approved by the Ethics Committee at the Shenzhen Institute of Advanced Technology, Chinese Academy of Sciences (Ethics Committee approval number: SIAT-IRB-200315-H0455), and written informed consent was obtained from all patients.

Results

The T_{1ρ}-weighted images (at TSL = 5 ms) from two volunteers using the TenSCOPE, L+S and LLR methods are shown in *Figures 2 and 3*. The estimated T_{1ρ} maps in selected ROIs are overlaid on the reconstructed images. The T_{1ρ}-weighted images reconstructed using the LLR method are more blurred than those using the other two methods, showing obvious smoothing artifacts. By adding the sparse component to the low-rank-based method, i.e., using the L+S method, the smoothing artifacts are alleviated. The T_{1ρ}-weighted images reconstructed using the TenSCOPE method show comparable image quality to the reference and achieve lower nRMSEs than images reconstructed using the L+S method for all acceleration factors. The T_{1ρ} maps estimated from the TenSCOPE reconstructions show good agreement with the reference estimated from the fully sampled acquisition. *Figure 4* shows the nRMSEs and MNADs of the selected ROIs (shown in *Figure 5*) from the accelerated reconstructions of the two datasets. The TenSCOPE reconstructions are more accurate than those obtained using the L+S and LLR methods, with the lowest nRMSE and MNAD values obtained for all acceleration factors. TenSCOPE improves the quality of the T_{1ρ} maps in terms of the MNAD relative to that of the L+S method, especially for high-acceleration cases.

Figure 6 shows the scatter plots and Bland-Altman plots of the mean T_{1ρ} values of ROIs using TenSCOPE compared with a reference. In the linear regression analyses, the estimated T_{1ρ} values using TenSCOPE show good agreement with the reference ($R^2 = 0.9554$ for 5.2× acceleration, $R^2 = 0.9213$ for 7.7× acceleration, and $R^2 = 0.9209$ for 9.7× acceleration). In the Bland-Altman analyses, the T_{1ρ} values agree well with the reference values for R=5.2 (T_{1ρ}: mean ± std: 40.4±1.4 ms, bias: 0.3 ms, 95% CI: -2.5, 3.1), R=7.7 (T_{1ρ}: mean ± std: 40.4± 2.1 ms, bias: 1.5 ms, 95% CI: -2.6, 5.6), and R=9.7 (T_{1ρ}: mean ± std: 40.9±2.2 ms, bias: 1.5 ms, 95% CI: -3.0, 5.9). No statistically significant differences were observed between the T_{1ρ} values measured across the subjects with different acceleration factors and the fully sampled reference.

Figure 7 shows the T_{1ρ}-weighted images obtained from the prospectively undersampled data using the TenSCOPE method for R=5 and R=7. Reference images are also shown for comparison. *Figure 8* shows the corresponding T_{1ρ} parameter maps estimated from the reconstructed images. The T_{1ρ} maps in the selected ROIs of cartilage regions were overlaid on the reconstructed T_{1ρ}-weighted images at TSL

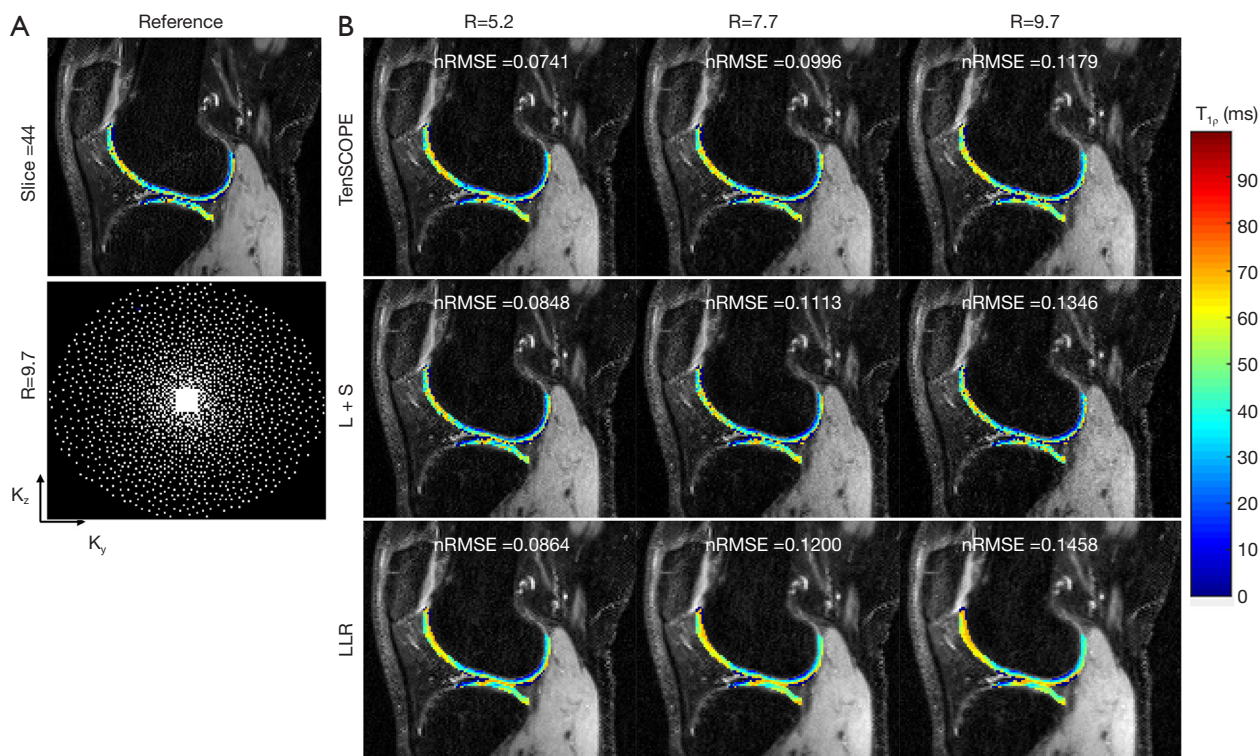


Figure 3 The undersampling pattern and estimated T_{1p} parameter maps for selected cartilage ROIs. (A) The 2D Poisson-disk random undersampling patterns in $ky-kz$ for a net acceleration factor $R=9.7$. (B) The estimated T_{1p} parameter maps for selected cartilage ROIs overlaid on the reconstructed T_{1p} -weighted images at $TSL=5$ ms for $R=5.2, 7.7,$ and 9.7 using the TenSCOPE, L+S, and LLR methods, respectively, for slice 44 of subject 2. The reference image and T_{1p} parameter map were obtained from the fully sampled k -space data. LLR, locally low-rank method; TSL, spin-lock time; ROI, region of interest.

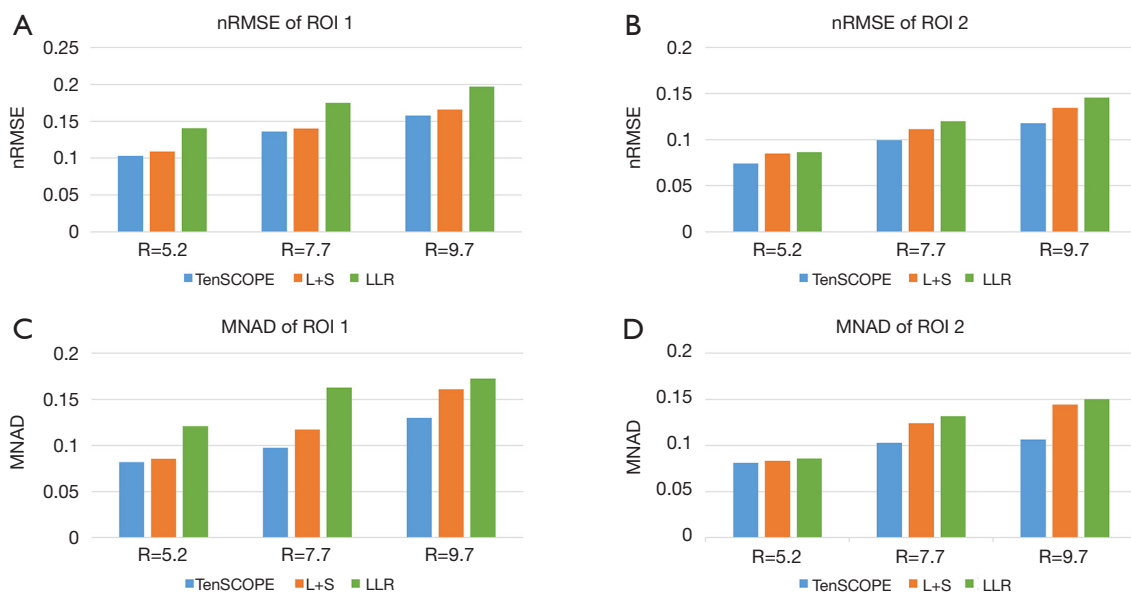


Figure 4 nRMSEs of the reconstructed images (A,B) and MNADs of the estimated T_{1p} parameter maps (C,D) for selected ROIs using the TenSCOPE, L+S and LLR methods at $R=5.2, 7.7$ and 9.7 , respectively. MNAD, median of the normalized absolute deviation; ROI, region of interest.

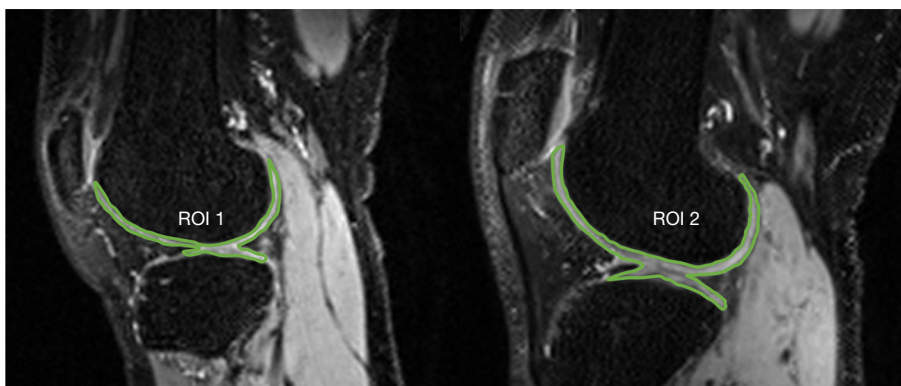


Figure 5 Selected ROIs of cartilage used for the nRMSE and MNAD evaluations in *Figure 4*. The numbers of voxels included in ROI 1 and ROI 2 are 216 and 305, respectively. MNAD, median of the normalized absolute deviation; ROI, region of interest.

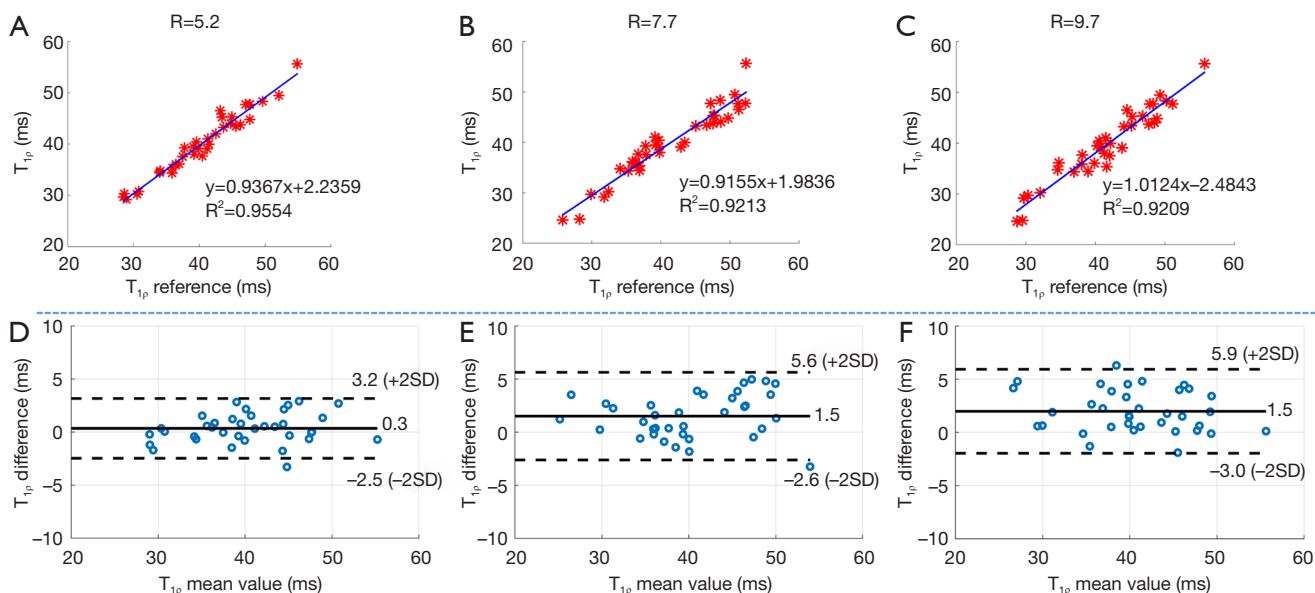


Figure 6 Linear regression (A,B,C) and Bland-Altman plots of the accelerated $T_{1\rho}$ parameters (D,E,F) with $R=5.2$, 7.7 , and 9.7 relative to the $T_{1\rho}$ parameters from the fully sampled reference. The solid and dashed lines in the Bland-Altman plots represent the bias and ± 2 standard deviation limits, respectively.

$=5$ ms. No obvious blurring artifacts were observed in the $T_{1\rho}$ -weighted images and $T_{1\rho}$ maps reconstructed using the TenSCOPE method for $R=5$ and $R=7$. The results of $T_{1\rho}$ values of the selected ROIs in cartilage regions shown in *Figure 8* and the Wilcoxon signed-rank test are shown in *Table 1*. There were no statistically significant differences between the $T_{1\rho}$ values measured by TenSCOPE for either accelerated scans ($R=5$, 7) or the reference values for the selected ROIs (both $P>0.05$).

Discussion

In this work, we developed a novel accelerated 3D $T_{1\rho}$ mapping of knee cartilage method to obtain the $T_{1\rho}$ parameters from highly undersampled data with the acceleration factor up to 9.7 . The signal-compensated robust tensor principal component analysis model for image reconstruction displayed excellent performance. According to our results, the reconstructed $T_{1\rho}$ -weighted images using TenSCOPE showed fewer blurring artifacts and achieved

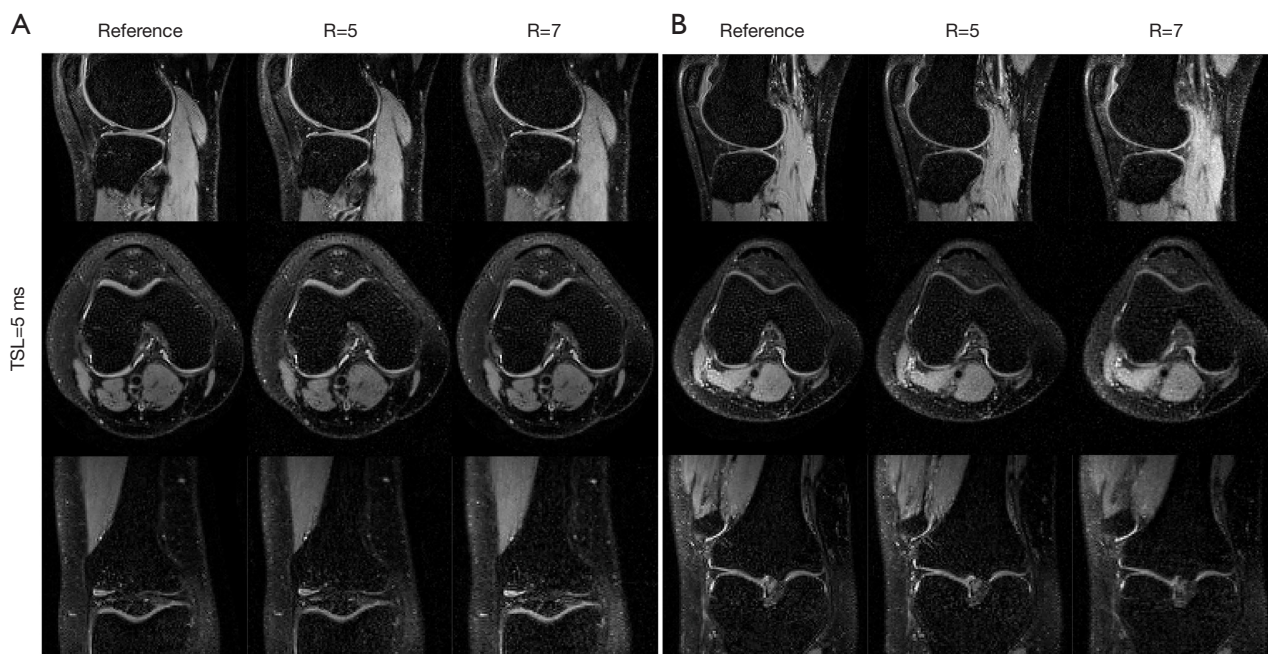


Figure 7 The reconstructed images at TSL=5 ms from the prospectively undersampled datasets of two subjects (A, subject 1, B, subject 2) for R=5 and R=7 using TenSCOPE. The reference images were obtained by applying the ESPIRiT method to the undersampled data with R=3. TSL, spin-lock time.

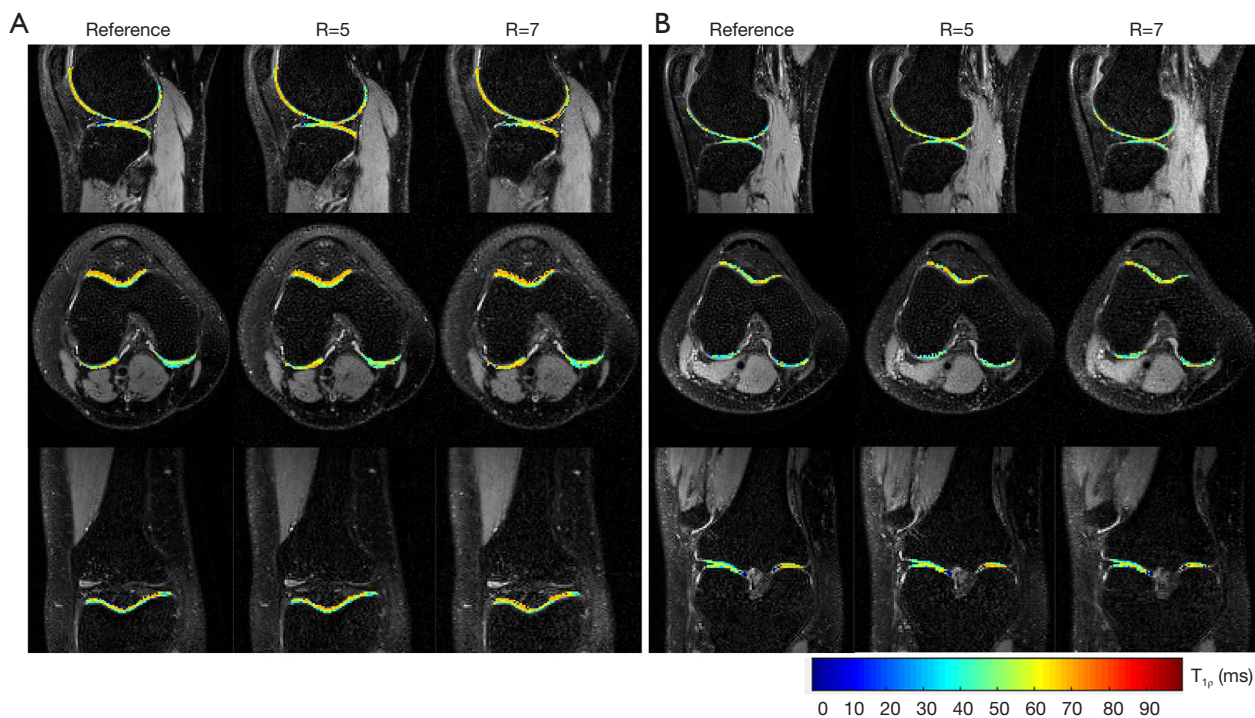


Figure 8 $T_{1\rho}$ maps estimated from the prospectively undersampled datasets of two subjects (A, subject 1, B, subject 2) for R=5 and R=7 using TenSCOPE. $T_{1\rho}$ parameter maps for selected cartilage ROIs are overlaid on the reconstructed $T_{1\rho}$ -weighted images at TSL =5 ms. The reference maps were obtained by applying the ESPIRiT method to the undersampled data with R=3. TSL, spin-lock time; ROI, region of interest.

Table 1 Average T_{1ρ} values of selected ROIs of cartilage regions in *Figure 8* obtained from reference scans and the accelerated acquisition with R=5 and 7, respectively, as well as the corresponding P value

	Reference	R=5	R=7
T _{1ρ} (ms)	54.0±2.9	53.9±3.6	53.8±4.0
P value	–	0.16	0.09

ROI, region of interest.

lower reconstruction errors than those obtained with other methods, i.e., the LLR method. Even at a high acceleration factor, the TenSCOPE method still maintains reasonable image quality and accurate T_{1ρ} maps. The resulting T_{1ρ} estimations show good agreement with the reference derived from the fully sampled data.

CS has been successful for accelerating T_{1ρ} mapping of knee cartilage. In Pandit *et al.* (14), a method which combined CS and autocalibrating reconstruction for Cartesian sampling (ARC) was applied to accelerate T_{1ρ} mapping of knee cartilage with acceleration factors up to 2.3. T_{1ρ} maps obtained from the retrospective reconstructions using this method were shown with errors less than 5%. In Zhou *et al.* (18), a combined reconstruction with locally adaptive iterative support detection (k-t LAISD) and PI was used to accelerate T_{1ρ} mapping of knee cartilage. The T_{1ρ} quantification results showed high fidelity between accelerated and fully sampled data with achieved acceleration factors of 3 and 3.5, due to the local adaptability of the regularization and joint estimation of the coil sensitivities. In the above two studies, no prospective undersampling was implemented and the sparse prior was mainly used. In Zibetti *et al.* (16), CS reconstruction using 12 different sparsifying transforms was compared in reducing the scan time of T_{1ρ} mapping for cartilage, and the low rank with spatial finite difference (L+S SFD) transform is suggested as one of the most suitable sparsifying transforms. In this work, we combined low-rank and sparse priors in the CS reconstruction and applied a signal-compensated robust tensor principal component analysis model to reconstruct 3D images from undersampled data. We provide comparable or better results compared with state-of-the-art CS methods. The prospective reconstructions showed that the proposed TenSCOPE method can achieve comparable performance to the reference scan using PI.

In our previous work (21), we showed that obvious blur artifacts were observed in the reconstructions using the low-rank-based methods such as LLR. By adding the

sparse component to the low-rank method, the smoothing artifacts were alleviated. The same conclusion can be drawn from *Figures 2* and *3*. Similar to the SCOPE method in our previous work, the sparse component in the proposed TenSCOPE method is the differentiation between the acquired images and the exponential relaxation model resulting from hardware imperfections of the MR scanner, noise, and other factors. The strength of the differentiation varies according to TSL, and it may be better to use different thresholds for the images at different TSLs. In previous studies (20,32), L+S decomposition was applied to dynamic imaging or multispectral imaging, in which the data did not fit a low-rank only component and therefore the sparse component contains significant energy. L+S decomposition was applied in static imaging in this study, but we found that some image details can still be observed in the sparse component, especially in the cartilage region. Therefore, although the energy (about 4.31% in average for our knee data) in the sparse component was relatively small, it could not be neglected in the reconstruction.

In our recent work (33), we applied the SCOPE method to reconstruct the T_{1ρ}-weighted images slice-by-slice in a 2D reconstruction version and showed the superiority of this method over the L+S method. In this study, we used a low-rank tensor to replace the low-rank matrix to capture the data correlation in multiple dimensions beyond the TSL direction. To validate the effectiveness of tensors in the reconstruction, we also compared TenSCOPE with SCOPE. *Figure 9* shows the reconstruction results using the proposed TenSCOPE and SCOPE methods. It can be observed that TenSCOPE improves the quality of the T_{1ρ}-weighted images and T_{1ρ} maps in terms of the nRMSE and MNAD relative to that of the SCOPE method, with lower nRMSEs and MNADs than SCOPE for all the acceleration factors.

In the proposed TenSCOPE method, the initial signal compensation coefficient was calculated from the center of fully sampled k-space data. The performance may be improved by adding a pre-reconstruction step; notably, the missing k-space data are interpolated using a TV-regularized estimate (34) prior to estimating the initial signal compensation coefficient. However, no such pre-reconstruction is necessary for the proposed method since the coefficient is updated iteratively in the reconstruction step. Four parameters, including the outer iteration number, inner iteration number, rank parameter for Tucker decomposition, and threshold for the sparse component, need to be carefully selected in the optimization process.

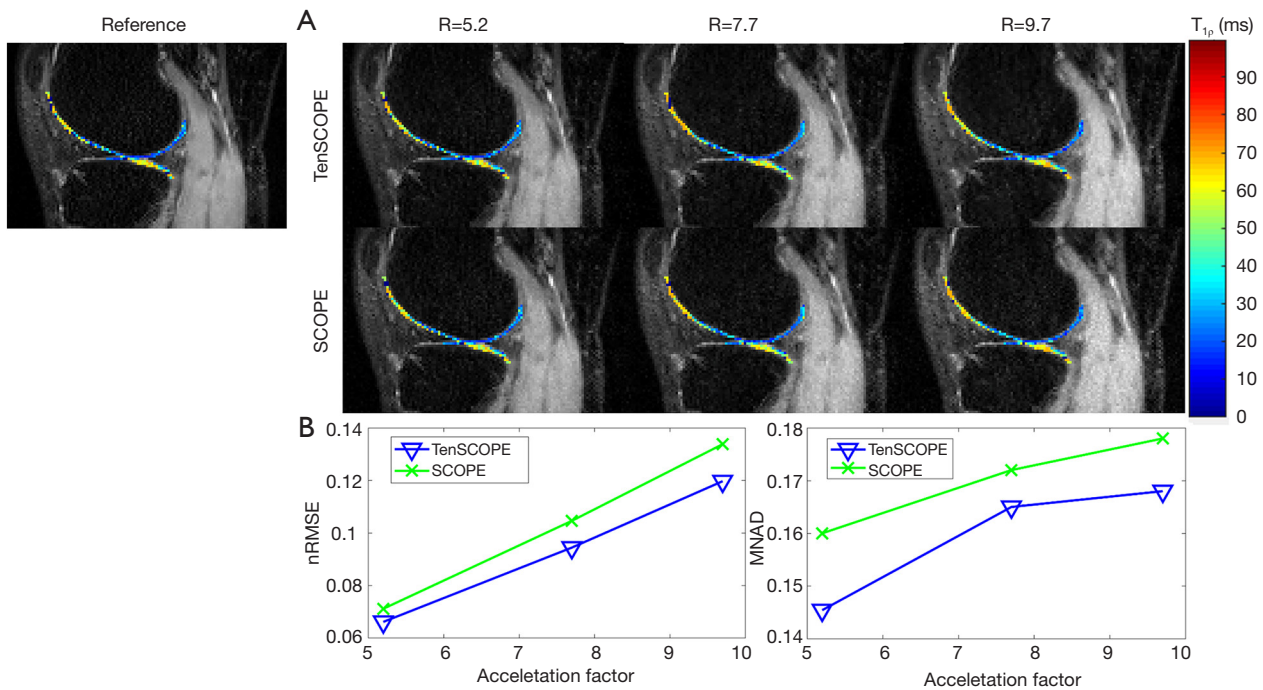


Figure 9 The estimated T_{1p} parameter maps for selected cartilage ROIs and the nRMSE curves of the selected ROI in the reconstructed T_{1p} -weighted images. (A) The estimated T_{1p} parameter maps for selected cartilage ROIs overlaid on the reconstructed T_{1p} -weighted images at TSL = 5 ms for R=5.2, 7.7, and 9.7 using the TenSCOPE and SCOPE methods for subject 3. (B) The nRMSE curves of the selected ROI in the reconstructed T_{1p} -weighted images using the TenSCOPE and SCOPE methods for all acceleration factors and the MNAD curves of the selected ROI in the reconstructed T_{1p} maps using the above two methods for all acceleration factors. TSL, spin-lock time; ROI, region of interest; MNAD, median of the normalized absolute deviation.

All the iteration numbers and the thresholds for the sparse component were selected empirically.

To evaluate the convergence of the proposed method, we calculated the relative change of image norm between two consecutive iterations at different undersampling levels with R=5.2, R=7.7 and R=9.7. The relative change was defined as

$$\text{norm}(I_{\text{iter}} - I_{\text{iter}-1}) / \text{norm}(I_{\text{iter}-1}) \quad [12]$$

where I_{iter} represents the reconstructed image in the iter-th iteration. The iteration number includes both the inner and outer iterations. *Figure 10* shows the relative change for the reconstructed image during each iteration. It demonstrates that the proposed algorithm converges with different undersampling levels as long as the iteration number is large enough. In this work, the algorithm iterates until the algorithm reaches the maximum number of iterations or the relative change in the solution is less than 5×10^{-4} .

The rank parameter for Tucker decomposition is an important parameter in the TenSCOPE method. *Figure 11*

shows an example of the reconstructed T_{1p} -weighted images with different rank parameters used in the Tucker decomposition at TSL = 5 ms for one slice of the dataset with R=7.7. While an insufficient tensor rank may lead to blurring artifacts or bias the T_{1p} measurements, high values can lead to limited noise reduction. Furthermore, the rank needs to be prespecified before running TenSCOPE. In this study, the rank parameter was selected empirically (30). An optimized rank parameter may help improve reconstruction performance (35). Regarding the regularization parameter for the sparse component, there is a trade-off between the convergence speed and the image quality. The algorithm converges more slowly using a small parameter, and more image details will be lost if a larger parameter is used, while the noise will not be sufficiently removed using a smaller parameter (*Figure 12*).

Since the T_{1p} map was updated in each outer iteration, Tucker decomposition was performed in each iteration, which further increased the computational burden of the proposed method. In our current implementation, the

computation was approximately 3 hours for each iteration for a data set size of 256 (frequency encoding) \times 146 (phase encoding) \times 124 (slices) \times 12 (channel) \times 5 (TSL). To reduce the reconstruction time, we applied parallel computing in MATLAB in the process of the $T_{1\rho}$ map estimation. The number of workers used in parallel computing is 30, and the

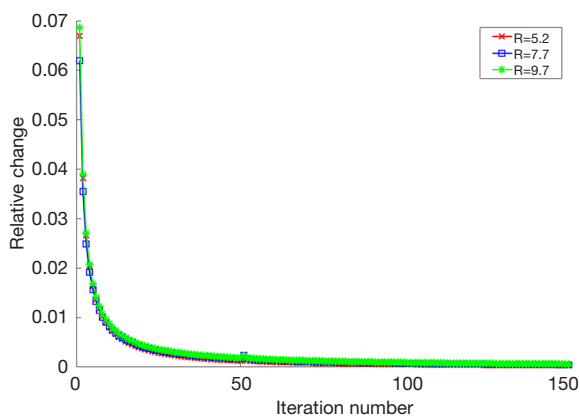


Figure 10 The relative change in TenSCOPE between the two consecutive iterations for the dataset of one volunteer with $R=5.2$, 7.7 and 9.7.

reconstruction times for $R=5.2$, 7.7, and 9.7 were 4.7, 6.8 and 8.5 hours, respectively. The reconstruction time of the TenSCOPE was longer than that of the L+S method and comparable to that of the LLR method. Taking $R=5$ as an example, the times required for L+S and LLR were 4.3 and 4.75 hours, respectively. The computational speed can be further improved by using a C implementation or graphical processing units (GPUs) instead of MATLAB.

PI can be integrated with CS-based methods to further accelerate the acquisition. In most CS-based fast MR parameter mapping methods, the fully sampled k-space center prolongs the acquisition time since multiple $T_{1\rho}$ -weighted images need to be acquired, especially in 3D $T_{1\rho}$ mapping applications. Therefore, PI can be used to undersample the k-space center to further reduce the acquisition time (36). For reconstruction, the undersampled k-space center can be first reconstructed with Generalized Autocalibrating Partial Parallel Acquisition (GRAPPA), and the proposed TenSCOPE method can then be used to reconstruct the $T_{1\rho}$ -weighted images.

This work lacks longitudinal reproducibility and variations in cartilage $T_{1\rho}$ studies. The longitudinal reproducibility and variations in cartilage $T_{1\rho}$ are necessary

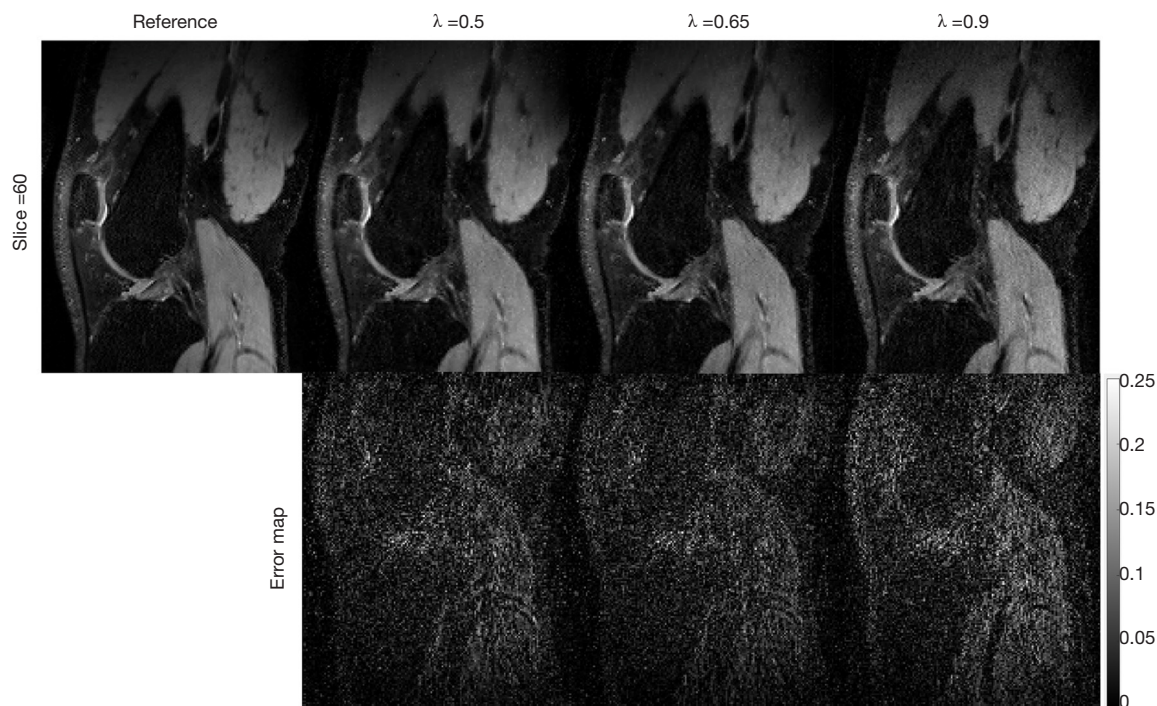


Figure 11 The reconstructed $T_{1\rho}$ -weighted images with different rank parameters (λ) used in the Tucker decomposition at TSL = 5 ms for one slice of the dataset with $R=7.7$. TSL, spin-lock time.

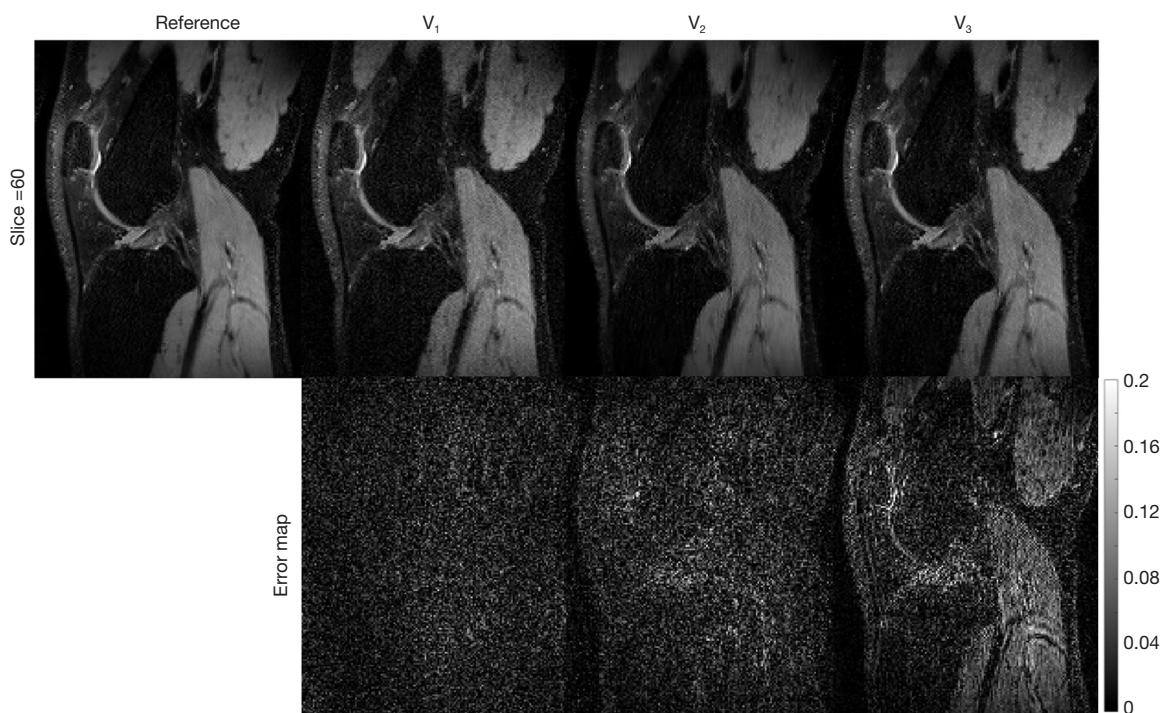


Figure 12 The reconstructed T_{1p} -weighted images at $TSL = 5$ ms with $R=5.2$ for one slice of the dataset with different threshold parameters for the sparse component $\{V_1=[0.001, 0.001, 0.002, 0.002, 0.002]$; $V_2=[0.01, 0.02, 0.02, 0.025, 0.025]$; $V_3=[0.1, 0.1, 0.2, 0.2, 0.2]\}$. TSL , spin-lock time.

in studies with clinical applications, such as cartilage degeneration evaluations. In future studies, longitudinal reproducibility assessments will be performed for clinical studies by applying the TenSCOPE method to detect early cartilage damage and degeneration in patients with OA, acute joint injury or cartilage damage.

Conclusions

We introduced a TenSCOPE method that uses a signal-compensated robust tensor principal component analysis model to reconstruct 3D images from undersampled data. The proposed method yields reasonable parameter estimates at high acceleration factors for the 3D T_{1p} mapping of *in vivo* knee cartilage, thereby reducing the scan time.

Acknowledgments

Funding: This work was partially supported by the National Key R&D Program of China Nos. 2020YFA0712200, 2017YFC0108802, National Natural Science Foundation of China under grant Nos. 61771463, 81830056, U1805261,

61671441 and 81971611, the Innovation and Technology Commission of the government of Hong Kong SAR under grant no. MRP/001/18X, the Key Laboratory for Magnetic Resonance and Multimodality Imaging of Guangdong Province under grant No. 2020B1212060051, and by the Chinese Academy of Sciences program under grant No. 2020GZL006.

Footnote

Conflicts of Interest: All authors have completed the ICMJE uniform disclosure form (available at <http://dx.doi.org/10.21037/qims-20-790>). DL serves as an unpaid Editorial Board Member of *Quantitative Imaging in Medicine and Surgery*. The other authors have no conflicts of interest to declare.

Ethical Statement: The authors are accountable for all aspects of the work in ensuring that questions related to the accuracy or integrity of any part of the work are appropriately investigated and resolved. The study was conducted in accordance with the Declaration of Helsinki

(as revised in 2013). The study was approved by the Ethics Committee at the Shenzhen Institute of Advanced Technology, Chinese Academy of Sciences (Ethics Committee approval number: SIAT-IRB-200315-H0455), and written informed consent was obtained from all patients.

Open Access Statement: This is an Open Access article distributed in accordance with the Creative Commons Attribution-NonCommercial-NoDerivs 4.0 International License (CC BY-NC-ND 4.0), which permits the non-commercial replication and distribution of the article with the strict proviso that no changes or edits are made and the original work is properly cited (including links to both the formal publication through the relevant DOI and the license). See: <https://creativecommons.org/licenses/by-nc-nd/4.0/>.

References

- Jinks C, Jordan K, Croft P. Osteoarthritis as a public health problem: the impact of developing knee pain on physical function in adults living in the community: (KNEST 3). *Rheumatology* 2007;46:877-81.
- Matzat SJ, van Tiel J, Gold GE, Oei EH. Quantitative MRI techniques of cartilage composition. *Quant Imaging Med Surg* 2013;3:162-74.
- Baboli R, Sharafi A, Chang G, Regatte RR. Isotropic morphometry and multicomponent T1 rho mapping of human knee articular cartilage in vivo at 3T. *J Magn Reson Imaging* 2018;48:1707-16.
- Koster IM, Oei EH, Hensen JH, Boks SS, Koes BW, Vroegindewij D, Hunink MG, Bierma-Zeinstra SM. Predictive factors for new onset or progression of knee osteoarthritis one year after trauma: MRI follow-up in general practice. *Eur Radiol* 2011;21:1509-16.
- Glyn-Jones S, Palmer AJ, Agricola R, Price AJ, Vincent TL, Weinans H, Carr AJ. Osteoarthritis. *Lancet* 2015;386:376-87.
- Baum T, Joseph GB, Karampinos DC, Jungmann PM, Link TM, Bauer JS. Cartilage and meniscal T2 relaxation time as non-invasive biomarker for knee osteoarthritis and cartilage repair procedures. *Osteoarthritis Cartilage* 2013;21:1474-84.
- Mosher TJ, Zhang Z, Reddy R, Boudhar S, Milestone BN, Morrison WB, Kwok CK, Eckstein F, Witschey WR, Borthakur A. Knee articular cartilage damage in osteoarthritis: analysis of MR image biomarker reproducibility in ACRIN-PA 4001 multicenter trial. *Radiology* 2011;258:832-42.
- Li X, Han ET, Ma CB, Link TM, Newitt DC, Majumdar S. In vivo 3T spiral imaging based multi-slice T(1rho) mapping of knee cartilage in osteoarthritis. *Magn Reson Med* 2005;54:929-36.
- Wáng YX, Zhang Q, Li X, Chen W, Ahuja A, Yuan J. T1ρ magnetic resonance: basic physics principles and applications in knee and intervertebral disc imaging. *Quant Imaging Med Surg* 2015;5:858-85.
- Li X, Majumdar S. Quantitative MRI of articular cartilage and its clinical applications. *J Magn Reson Imaging* 2013;38:991-1008.
- Bolbos RI, Zuo J, Banerjee S, Link TM, Ma CB, Li XJ, Majumdar S. Relationship between trabecular bone structure and articular cartilage morphology and relaxation times in early OA of the knee joint using parallel MRI at 3 T. *Osteoarthritis Cartilage* 2008;16:1150-9.
- Li X, Benjamin Ma C, Link TM, Castillo DD, Blumenkrantz G, Lozano J, Carballido-Gamio J, Ries M, Majumdar S. In vivo T(1rho) and T(2) mapping of articular cartilage in osteoarthritis of the knee using 3 T MRI. *Osteoarthritis Cartilage* 2007;15:789-97.
- Stahl R, Luke A, Li XJ, Carballido-Gamio J, Ma CB, Majumdar S, Link TM. T1rho, T2 and focal knee cartilage abnormalities in physically active and sedentary healthy subjects versus early OA patients--a 3.0-Tesla MRI study. *Eur Radiol* 2009;19:132-43.
- Pandit P, Rivoire J, King K, Li X. Accelerated T1ρ acquisition for knee cartilage quantification using compressed sensing and data-driven parallel imaging: A feasibility study. *Magn Reson Med* 2016;75:1256-61.
- Zibetti MVW, Baboli R, Chang G, Otazo R, Regatte RR. Rapid compositional mapping of knee cartilage with compressed sensing MRI. *J Magn Reson Imaging* 2018;48:1185-98.
- Zibetti MVW, Sharafi A, Otazo R, Regatte RR. Accelerating 3D-T 1ρ mapping of cartilage using compressed sensing with different sparse and low rank models. *Magn Reson Med* 2018;80:1475-91.
- Zibetti MVW, Sharafi A, Otazo R, Regatte RR. Compressed sensing acceleration of biexponential 3D-T 1ρ relaxation mapping of knee cartilage. *Magn Reson Med* 2019;81:863-80.
- Zhou Y, Pandit P, Pedoia V, Rivoire J, Wang Y, Liang D, Li X, Ying L. Accelerating T1ρ cartilage imaging using compressed sensing with iterative locally adapted support detection and JSENSE. *Magn Reson Med* 2016;75:1617-29.

19. Zibetti MVW, Sharafi A, Otazo R, Regatte RR. Accelerated mono- and biexponential 3D-T1 ρ relaxation mapping of knee cartilage using golden angle radial acquisitions and compressed sensing. *Magn Reson Med* 2020;83:1291-309.
20. Otazo R, Candes E, Sodickson DK. Low-Rank Plus Sparse Matrix Decomposition for Accelerated Dynamic MRI with Separation of Background and Dynamic Components. *Magn Reson Med* 2015;73:1125-36.
21. Zhu Y, Liu Y, Ying L, Peng X, Wang YJ, Yuan J, Liu X, Liang D. SCOPE: signal compensation for low-rank plus sparse matrix decomposition for fast parameter mapping. *Phys Med Biol* 2018;63:185009.
22. Roohi SF, Zonoobi D, Kassim AA, Jaremko JL. Multi-dimensional low rank plus sparse decomposition for reconstruction of under-sampled dynamic MRI. *Pattern Recognition* 2017;63:667-79.
23. Liu Y, Liu T, Liu J, Zhu C. Smooth robust tensor principal component analysis for compressed sensing of dynamic MRI. *Pattern Recognition* 2020;102:107252.
24. Pruessmann KP, Weiger M, Bornert P, Boesiger P. Advances in sensitivity encoding with arbitrary k-space trajectories. *Magn Reson Med* 2001;46:638-51.
25. De Lathauwer L, De Moor B, Vandewalle J. On the best rank-1 and rank-(R1, R2,...,RN) approximation of higher-order tensor. *SIAM Journal on Matrix Analysis and Applications* 2000;21:1324-42.
26. Ying JX, Lu HF, Wei QT, Cai JF, Guo D, Wu JH, Chen Z, Qu XB. Hankel Matrix Nuclear Norm Regularized Tensor Completion for N-dimensional Exponential Signals. *IEEE Trans Signal Process* 2017;65:3702-17.
27. Long Z, Liu YP, Chen LX, Zhu C. Low rank tensor completion for multiway visual data. *Signal Processing* 2019;155:301-16.
28. Mitrea BG, Krafft AJ, Song R, Loeffler RB, Hillenbrand CM. Paired self-compensated spin-lock preparation for improved T1 ρ quantification. *J Magn Reson* 2016;268:49-57.
29. Uecker M, Lai P, Murphy MJ, Virtue P, Elad M, Pauly JM, Vasanawala SS, Lustig M. ESPIRiT--an eigenvalue approach to autocalibrating parallel MRI: where SENSE meets GRAPPA. *Magn Reson Med* 2014;71:990-1001.
30. Cao W, Wang Y, Sun J, Meng D, Yang C, Cichocki A, Xu Z. Total Variation Regularized Tensor RPCA for Background Subtraction From Compressive Measurements. *IEEE Trans Image Process* 2016;25:4075-90.
31. Zhang T, Pauly JM, Levesque IR. Accelerating parameter mapping with a locally low rank constraint. *Magn Reson Med* 2015;73:655-61.
32. Levine E, Stevens K, Beaulieu C, Hargreaves B. Accelerated three-dimensional multispectral MRI with robust principal component analysis for separation of on- and off-resonance signals. *Magn Reson Med* 2018;79:1495-505.
33. Liu Y, Chen W, Liu X, Zheng H, Liang D, Zhu Y. Accelerating 3D-T1 ρ Cartilage imaging using signal compensated low-rank plus sparse matrix decomposition. In Proceedings of the 28th Annual Meeting of ISMRM, Virtual Conference, 2020. Abstract 2744.
34. Yang JF, Zhang Y, Yin WT. A Fast Alternating Direction Method for TVL1-L2 Signal Reconstruction From Partial Fourier Data. *IEEE Journal of Selected Topics in Signal Processing* 2010;4:288-97.
35. Yaman B, Weingartner S, Kargas N, Sidiropoulos ND, Akcakaya M. Low-Rank Tensor Models for Improved Multi-Dimensional MRI: Application to Dynamic Cardiac T1 Mapping. *IEEE Trans Comput Imaging* 2019;6:194-207.
36. Zhu Y, Liu Y, Ying L, Qiu Z, Liu Q, Jia S, Wang H, Peng X, Liu X, Zheng H, Liang D. A 4-minute solution for submillimeter whole-brain T1 ρ quantification. *Magn Reson Med* 2021;85:3299-307.

Cite this article as: Liu Y, Ying L, Chen W, Cui ZX, Zhu Q, Liu X, Zheng H, Liang D, Zhu Y. Accelerating the 3D T ρ mapping of cartilage using a signal-compensated robust tensor principal component analysis model. *Quant Imaging Med Surg* 2021;11(8):3376-3391. doi: 10.21037/qims-20-790